MSR scheme: *R*-scale behavior in the inclusive and differential case

Theory-Experimental Top Quark Mass Workshop

Toni Mäkelä
28.6.2022

HELMHOLTZ RESEARCH FOR GRAND CHALLENGES

DESY.

The renormalization of the top quark mass

- A precise understanding of quark masses is important for a precise understanding of the standard model

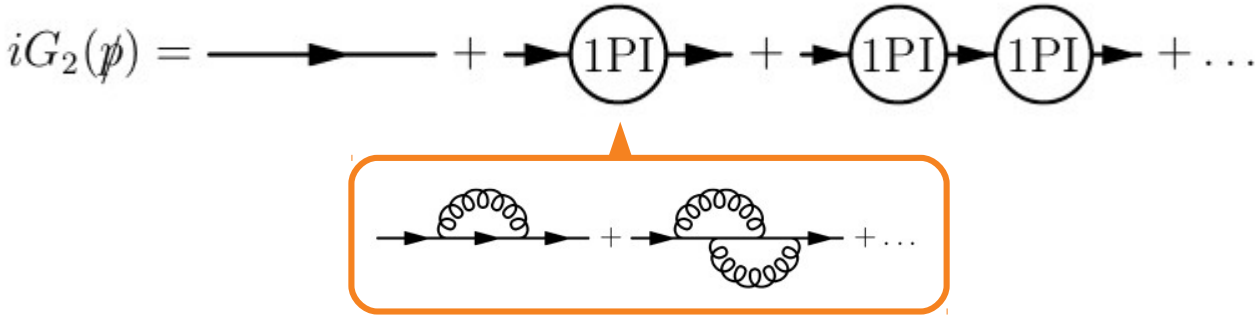

- However, quarks are not observed as free particles, and their masses are defined formally via renormalization. E.g. two common options:
  - **The pole scheme** (pQCD equivalent of the on-shell mass of a free particle)
  - **The $\overline{\mathrm{MS}}$ scheme** (theoretical advantages)
- Although theoretically well-defined masses can be extracted from cross sections, there are long-standing discussions e.g. on how to interpret / calibrate the Monte Carlo mass parameter
  - The **MSR** mass has stirred interest in the theory and experimental communities

The MSR and $\overline{\mathrm{MS}}$ schemes

- The pole and $\overline{\mathrm{MS}}$ masses are related by

$$m_{\mathrm{t}}^{\mathrm{pole}} = \overline{m}_{\mathrm{t}}(\mu_m)\left(1 + \sum_{n=1} \frac{\alpha_S(\mu_m)^n}{\pi^n} d_n(\mu_m)\right)$$

- The MSR mass introduces a mass renormalization scale R and approaches the pole mass for $R \to 0$, and the $\overline{\mathrm{MS}}$ mass for $R \to \overline{m}_{\mathrm{t}}(\overline{m}_{\mathrm{t}})$

$$m_{\mathrm{t}}^{\mathrm{pole}} = m_{\mathrm{t}}^{\mathrm{MSR}} + R \sum_{n=1} \frac{\alpha_S(R)^n}{\pi^n} d_n^{\mathrm{MSR}}(R)$$

Two ways to define the MSR mass lead to different decoupling coefficients

- Integrating the top quark out for scales below $\overline{m}_{\mathrm{t}}$
  - *Natural MSR* (**MSRn**)
- Rewriting $\alpha_S^{(5+1)}$ in terms of $\alpha_S^{(5)}$
  - *Practical MSR* (**MSRp**)

Running

- The MSR mass is mostly expected to be applied at mass scales below the $\overline{\mathrm{MS}}$ mass

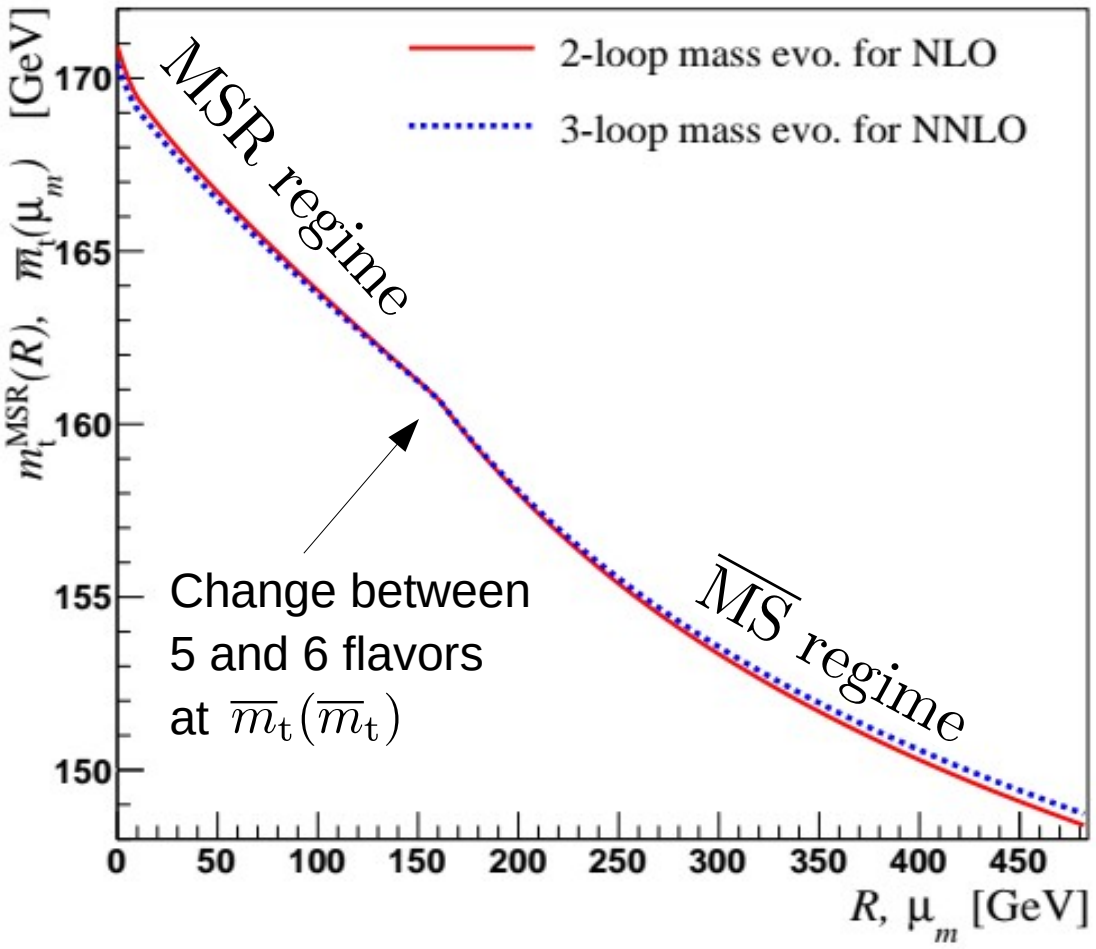

The single-differential $t\bar{t}$ cross section at NLO

- The cross section in running mass schemes is divided into the LO, NLO and derivative contributions. The MCFM implementation can also provide each term individually, allowing more in-depth studies of the behavior of the cross section as a function of the scales μ_r, μ_f and *R* (or μ_m), *independent of each other!*

- In the MSR regime $(R < \overline{m}_\mathrm{t}(\overline{m}_\mathrm{t}))$

$$\frac{d\sigma}{dX} = a_S(\mu_r)^2 \frac{d\sigma^{(0)}}{dX}\left(m_\mathrm{t}^\mathrm{MSR}(R), \mu_r\right) + a_S(\mu_r)^3 \frac{d\sigma^{(1)}}{dX}\left(m_\mathrm{t}^\mathrm{MSR}(R), \mu_r\right) + a_S(\mu_r)^3 d_1 R \frac{d}{dm_\mathrm{t}}\left(\frac{d\sigma^{(0)}(m_\mathrm{t}, \mu_r)}{dX}\right)\Bigg|_{m_\mathrm{t}=m_\mathrm{t}^\mathrm{MSR}(R)}$$

- In the $\overline{\mathrm{MS}}$ regime $(\mu_m > \overline{m}_\mathrm{t}(\overline{m}_\mathrm{t}))$

$$\frac{d\sigma}{dX} = a_S(\mu_r)^2 \frac{d\sigma^{(0)}}{dX}\left(\overline{m}_\mathrm{t}(\mu_m), \mu_r\right) + a_S(\mu_r)^3 \frac{d\sigma^{(1)}}{dX}\left(\overline{m}_\mathrm{t}(\mu_m), \mu_r\right) + a_S(\mu_r)^3 d_1(\mu_m)\overline{m}_\mathrm{t}(\mu_m) \frac{d}{dm_\mathrm{t}}\left(\frac{d\sigma^{(0)}(m_\mathrm{t}, \mu_r)}{dX}\right)\Bigg|_{m_\mathrm{t}=\overline{m}_\mathrm{t}(\mu_m)}$$

Inclusive cross section

- As a first test, the inclusive $t\bar{t}$ production cross section obtained from MCFM agrees with previous NLO results from HATHOR
- All differences are within the numerical uncertainties of MCFM
- Next: the contributions of the LO, NLO (real & virtual) and derivative terms obtained from the MCFM implementation can be compared to an external computation constructing a numerical stencil out of standard MCFM pole scheme results

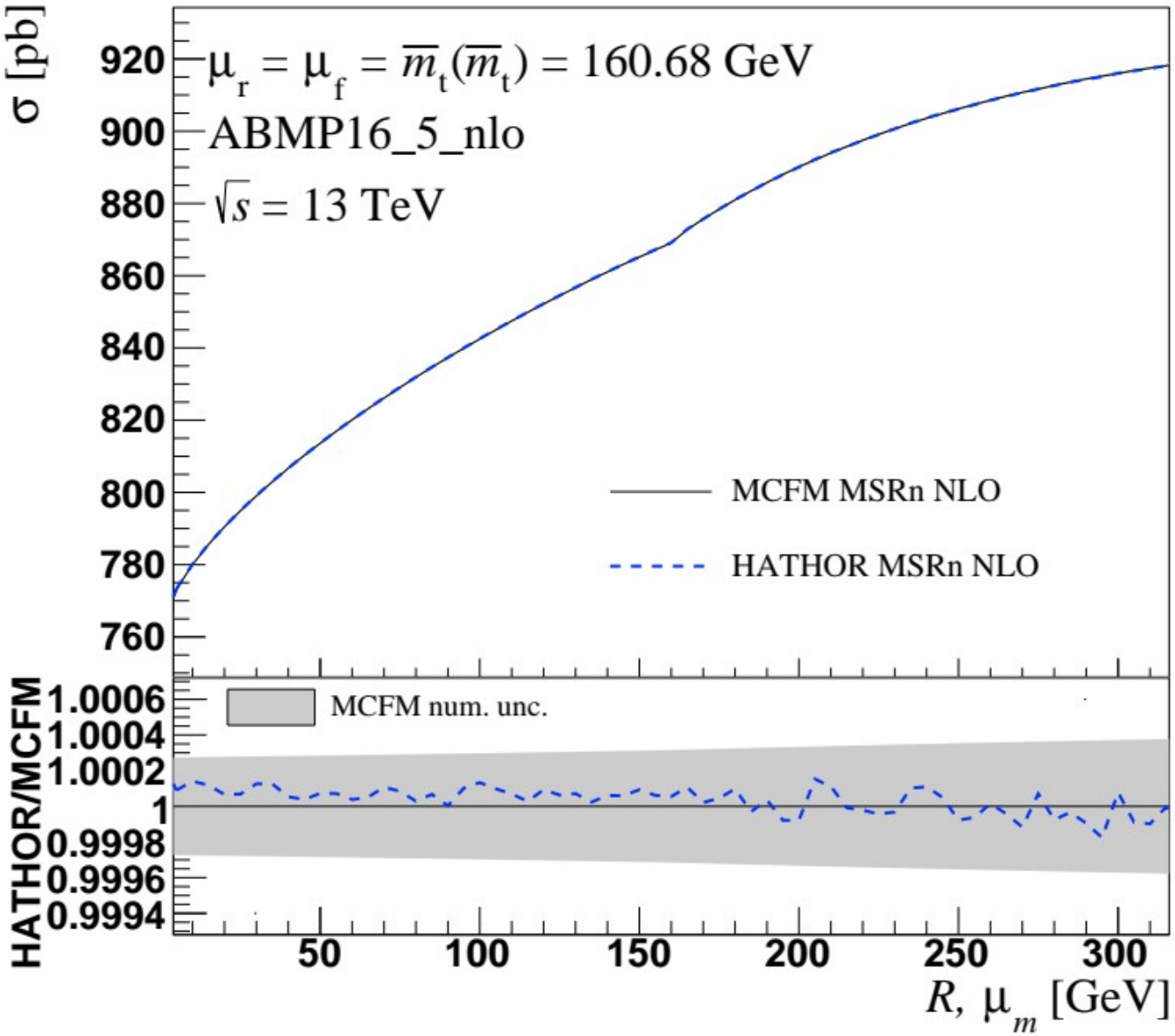

Validation of the MCFM v6.8 implementation

Comparison to an external computation

- The contributions of the LO, NLO (real & virtual) and derivative terms obtained from the MCFM implementation can be compared to an external computation constructing a numerical stencil out of standard MCFM pole scheme results

$m_{t\bar{t}}$

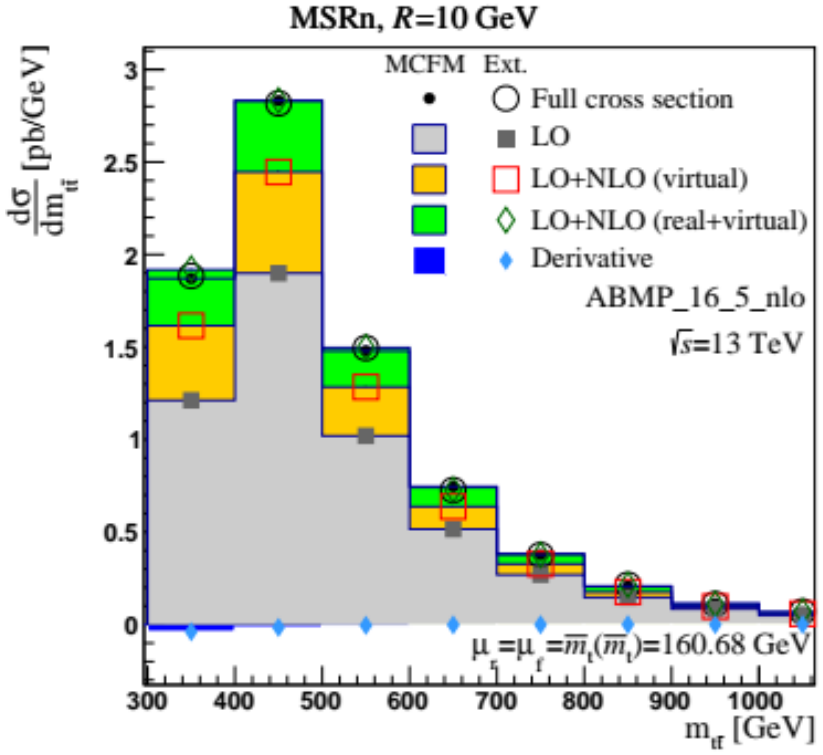

$p_T(\bar{t})$

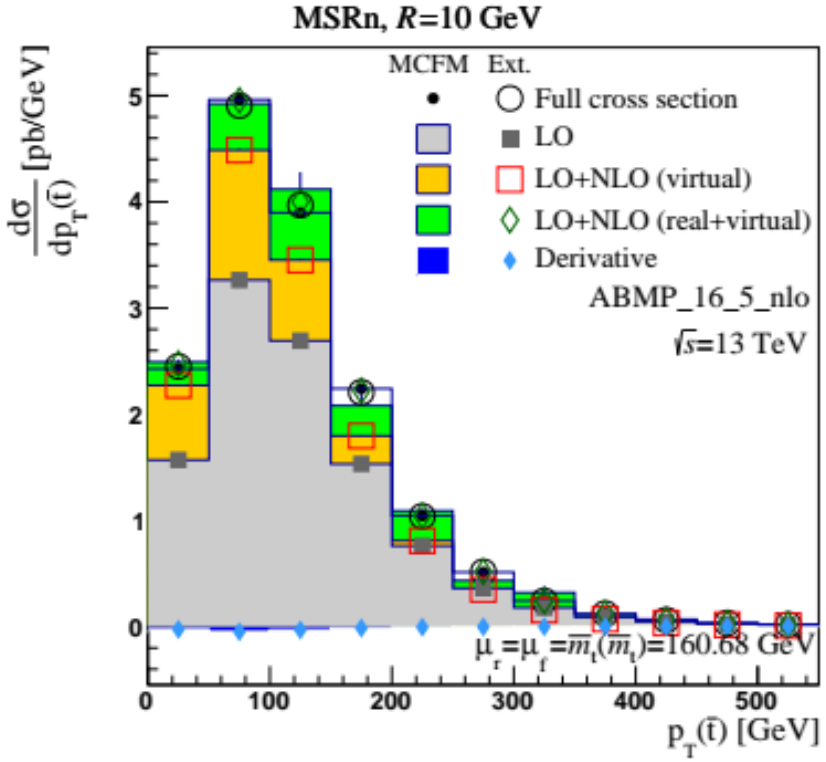

$y(\bar{t})$

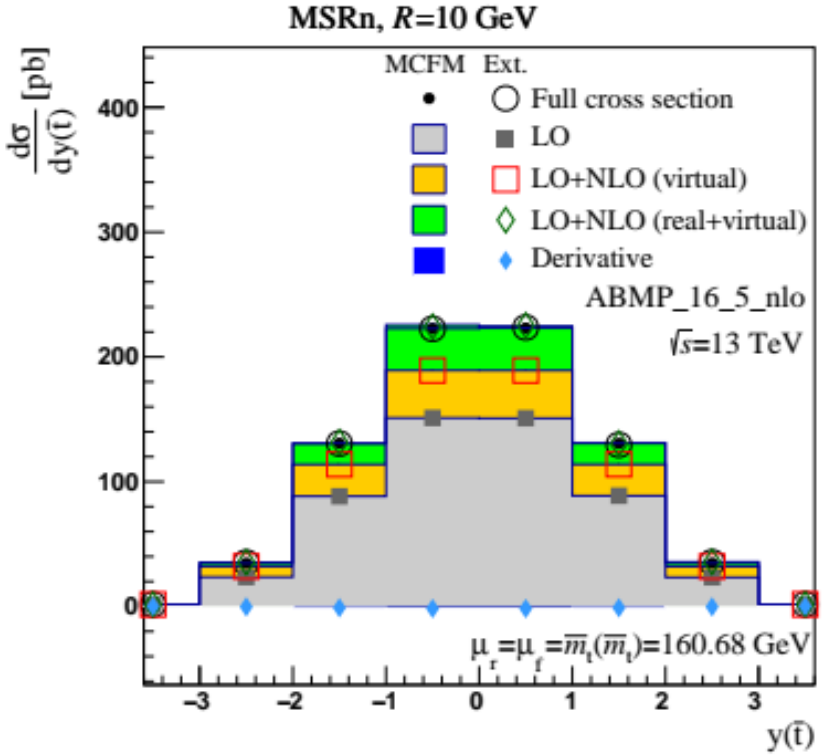

Validation of the MCFM v6.8 implementation

Comparison to an external computation

- The contributions of the LO, NLO (real & virtual) and derivative terms obtained from the MCFM implementation can be compared to an external computation constructing a numerical stencil out of standard MCFM pole scheme results

$m_{t\bar{t}}$

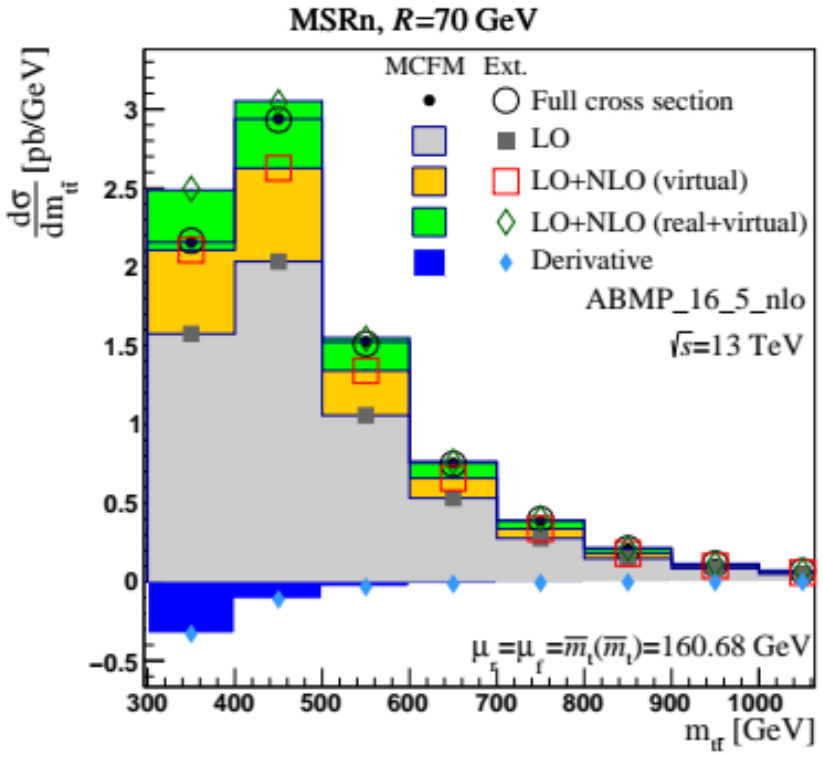

$p_{\mathrm{T}}(\bar{\mathrm{t}})$

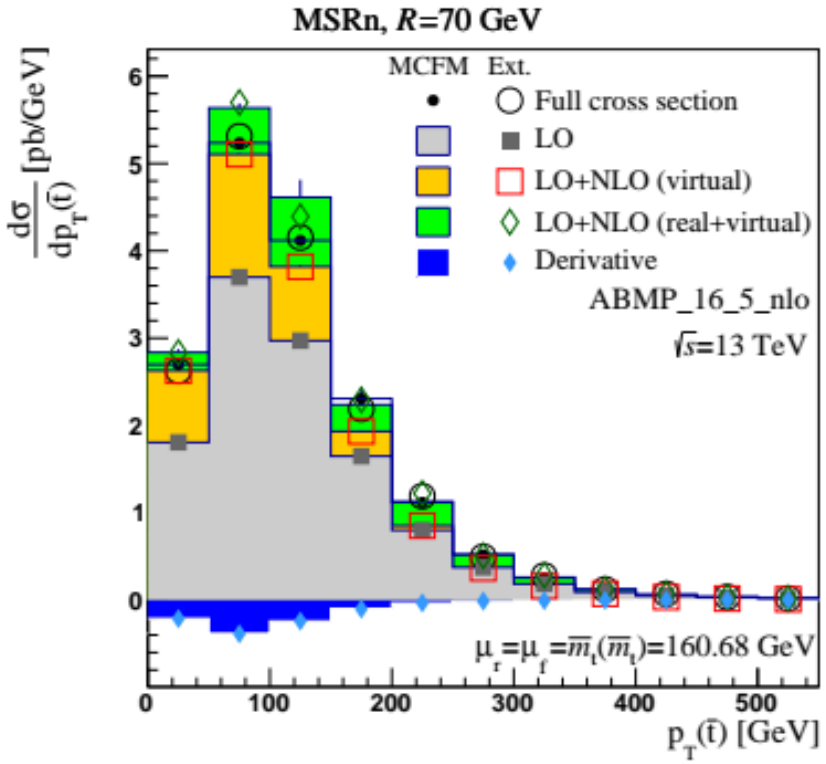

$y(\bar{\mathrm{t}})$

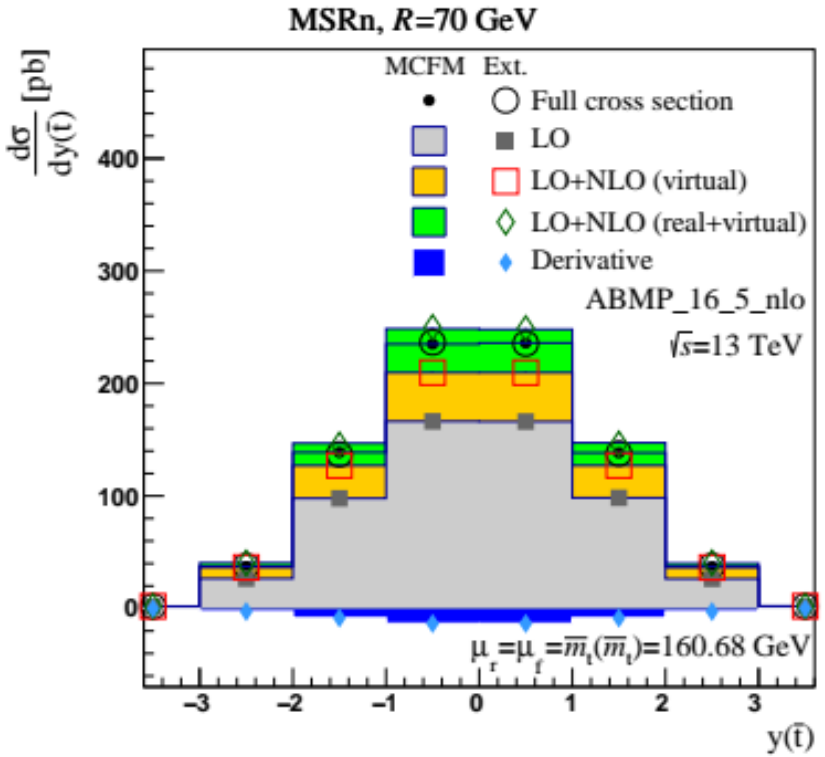

Validation of the MCFM v6.8 implementation

Comparison to an external computation

- The contributions of the LO, NLO (real & virtual) and derivative terms obtained from the MCFM implementation can be compared to an external computation constructing a numerical stencil out of standard MCFM pole scheme results

$m_{t\bar{t}}$

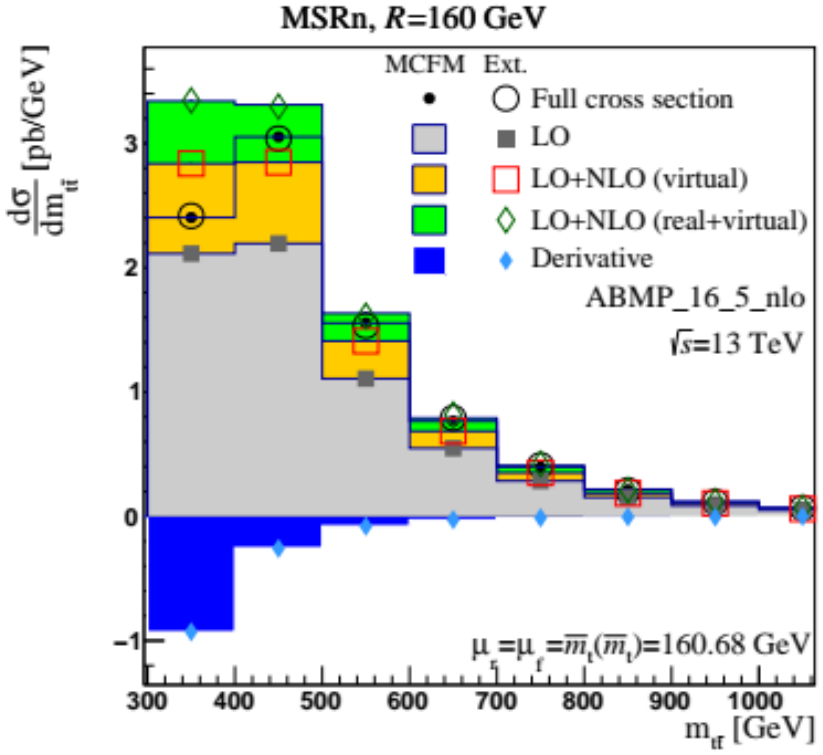

$p_T(\bar{t})$

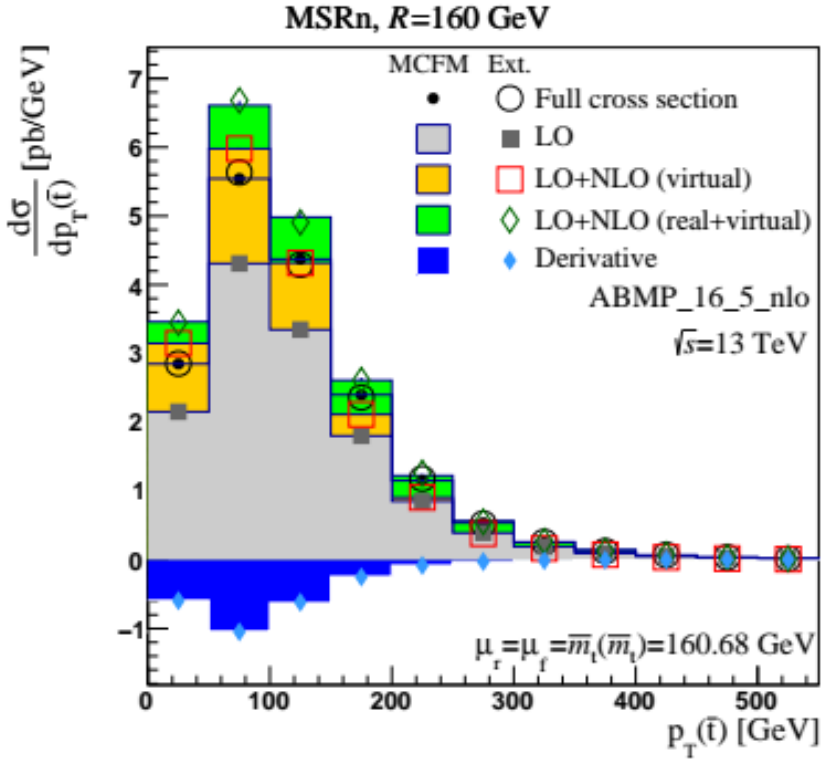

$y(\bar{t})$

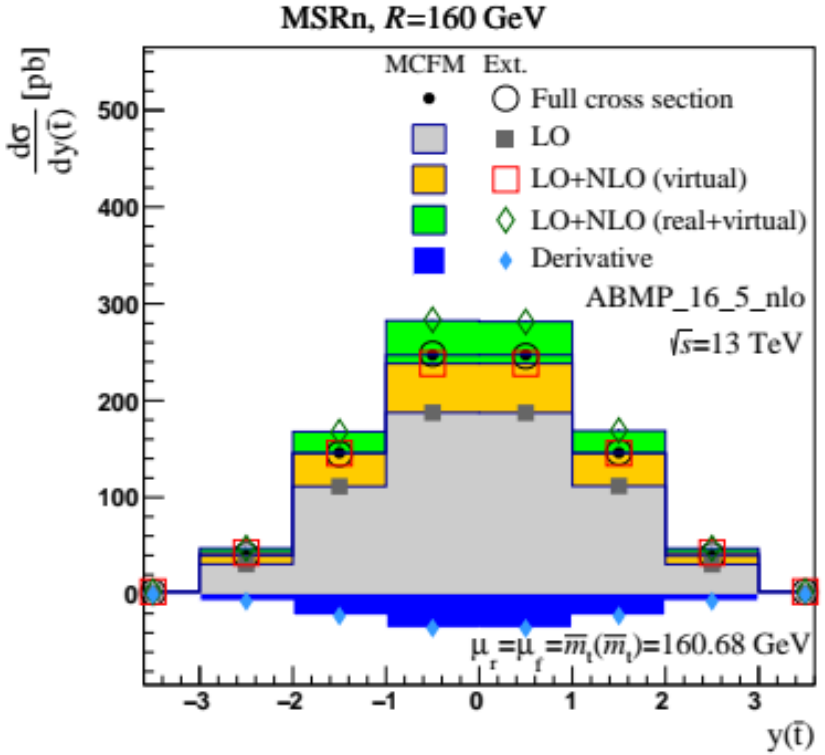

Validation of the MCFM v6.8 implementation

Comparison to an external computation

- The contributions of the LO, NLO (real & virtual) and derivative terms obtained from the MCFM implementation can be compared to an external computation constructing a numerical stencil out of standard MCFM pole scheme results

$m_{t\bar{t}}$

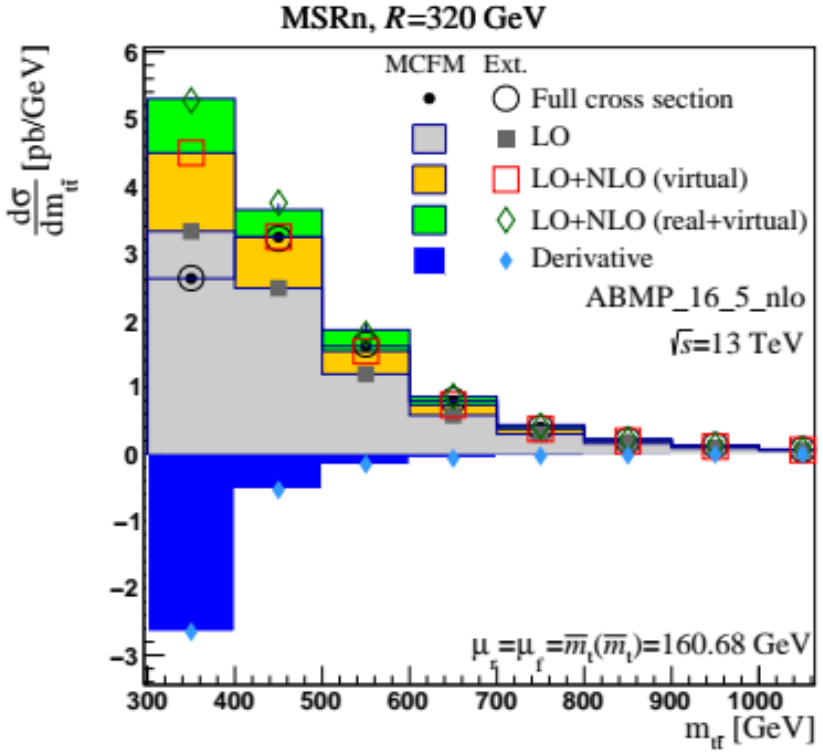

$p_T(\bar{t})$

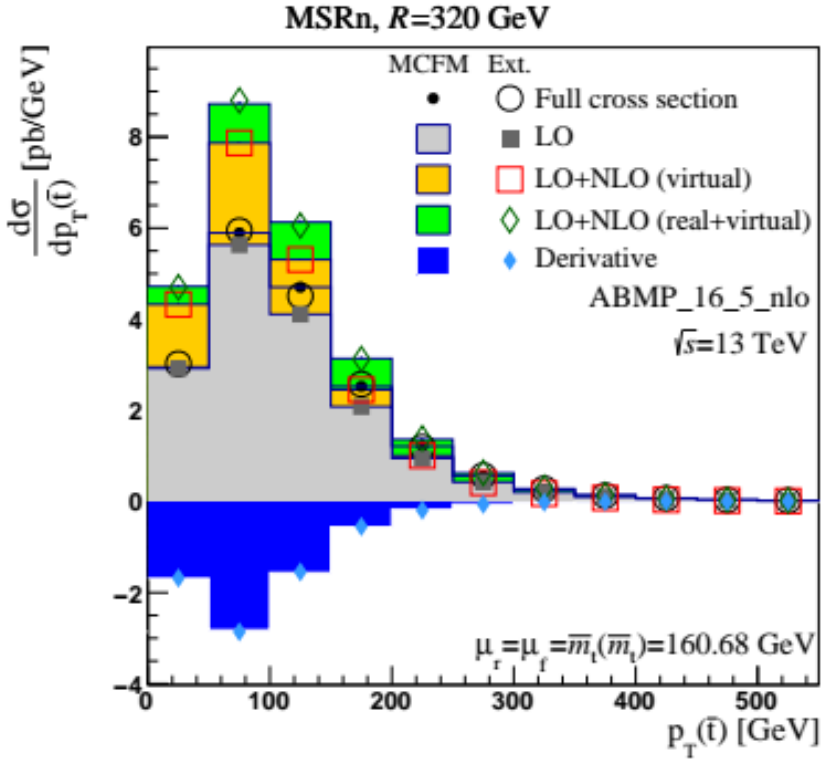

$y(\bar{t})$

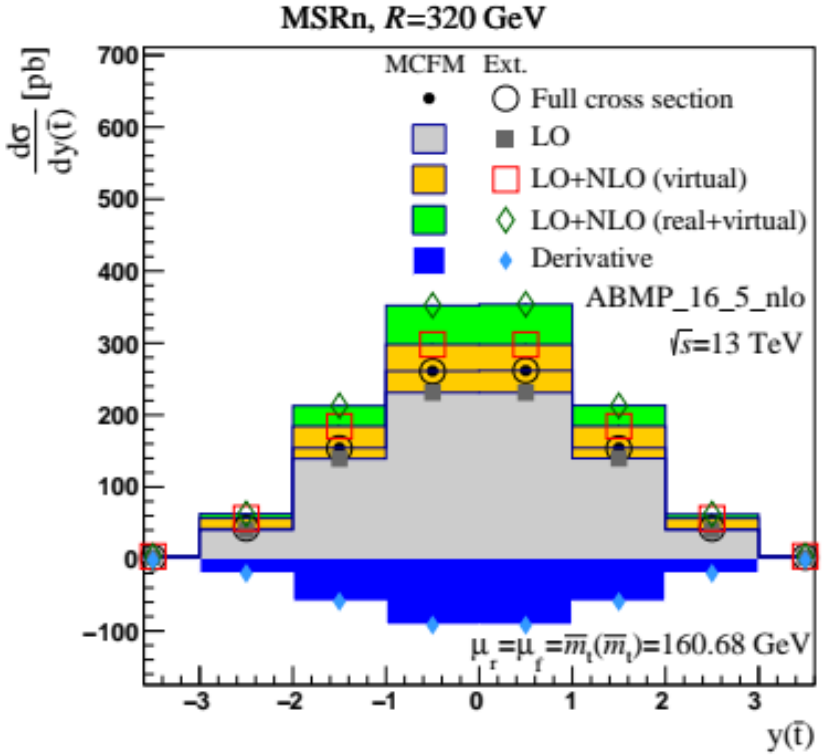

Studies of μ_r, μ_f and *R* behavior in $d\sigma/dm_{t\bar{t}}$ at NLO

- The $d\sigma/dm_{t\bar{t}}$ distribution is investigated more thoroughly via a fine binning
- Negative cross sections at the threshold are attributed to missing Coulomb corrections
  - The derivative term is negative, decreases more rapidly than the other positive contributions increase
- Next: let's look at the cross section in a single bin as a function of the mass scale
  - Especially the bins near the peak are interesting: sensitivity to the mass

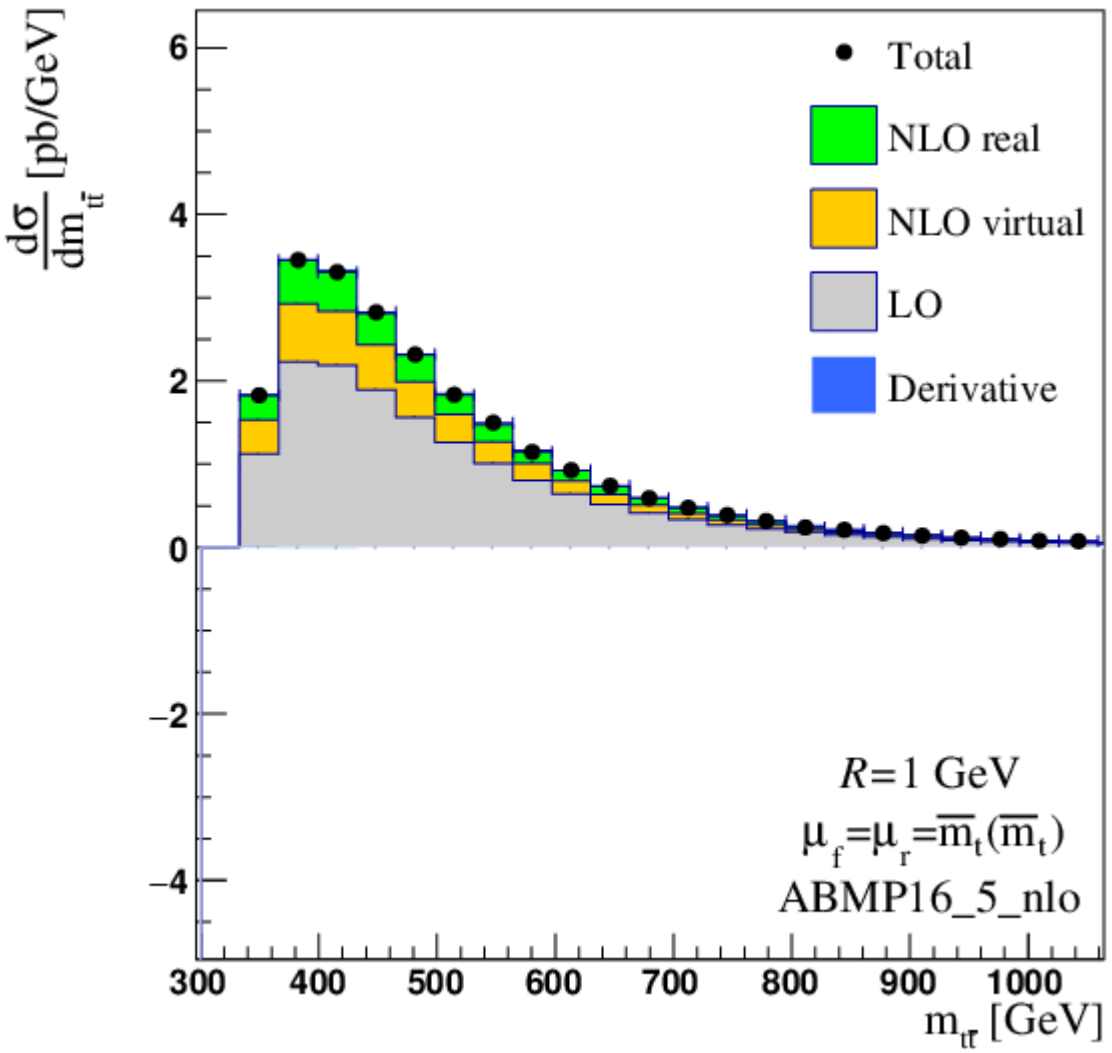

Studies of μ_r, μ_f and *R* behavior in $d\sigma/dm_{t\bar{t}}$ at NLO

- Investigating the effect of the central choice of μ_r, μ_f via the cross sections per bin, as a function of the mass scale
- Lower scale values seem to stabilize the NLO cross section as a function of *R*, the effect is particularly important for the lowest bins

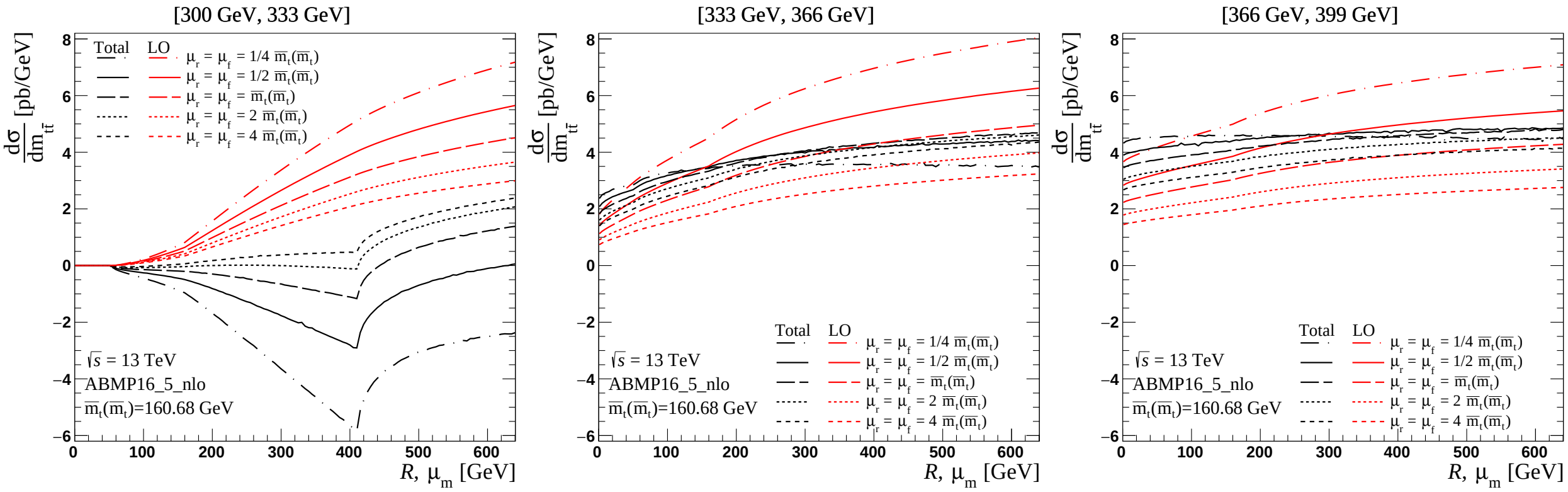

Studies of μ_r, μ_f and *R* behavior in $d\sigma/dm_{t\bar{t}}$ at NLO

- Investigating the effect of the central choice of μ_r, μ_f via the cross sections per bin, as a function of the mass scale ⟶ also look at the LO vs NLO ratios
- Lower scale values seem to stabilize the NLO cross section as a function of *R*, the effect is particularly important for the lowest bins

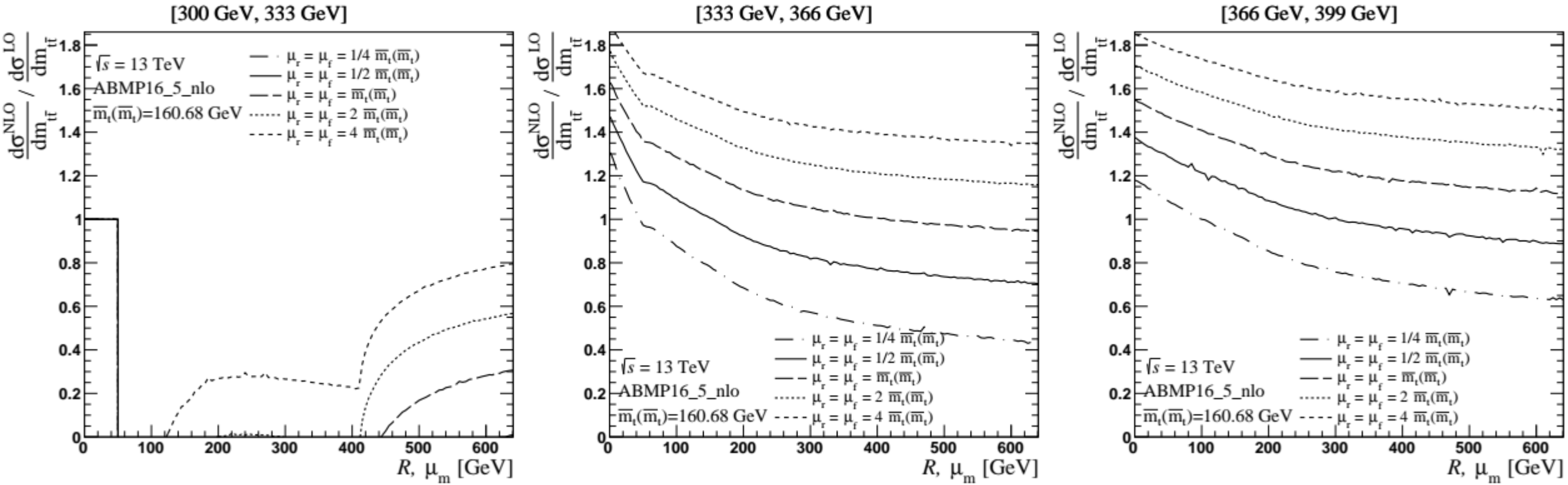

Studies of μ_r, μ_f and *R* behavior in $d\sigma/dm_{t\bar{t}}$ at NLO

- With the fine binning, the two lowest lowest $m_{t\bar{t}}$ bins indicate the regions suffering from missing Coulomb corrections

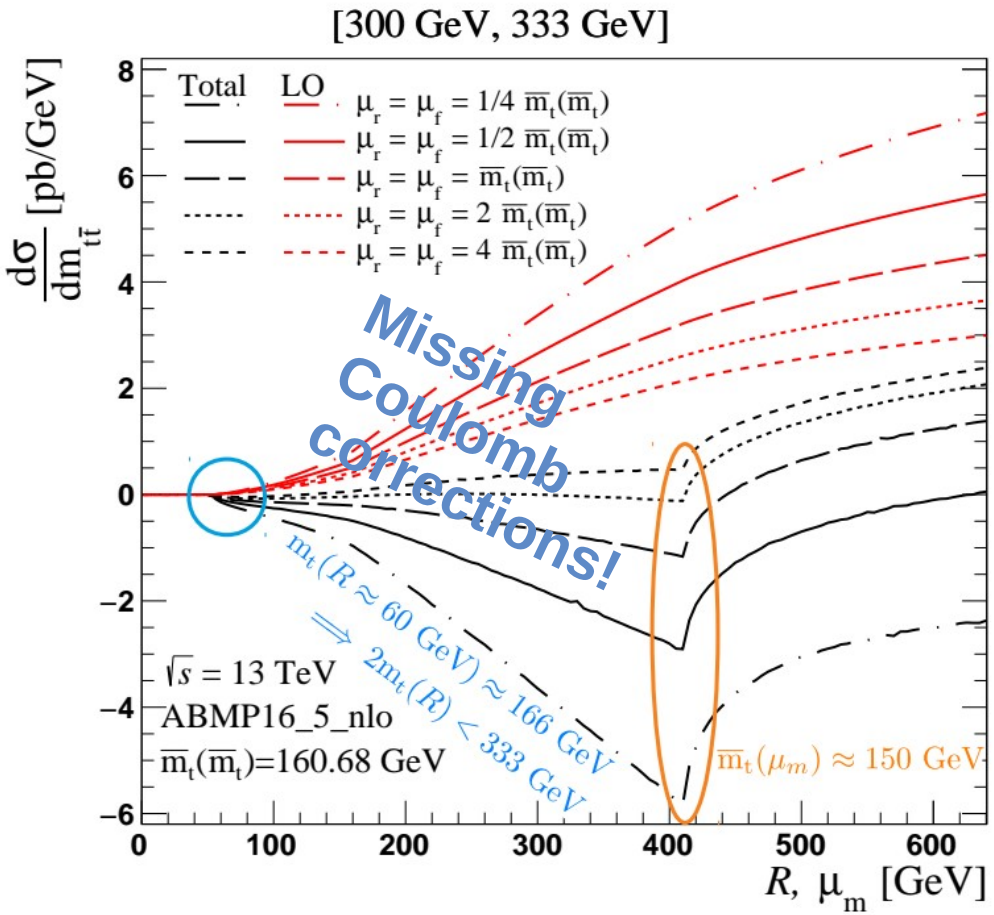

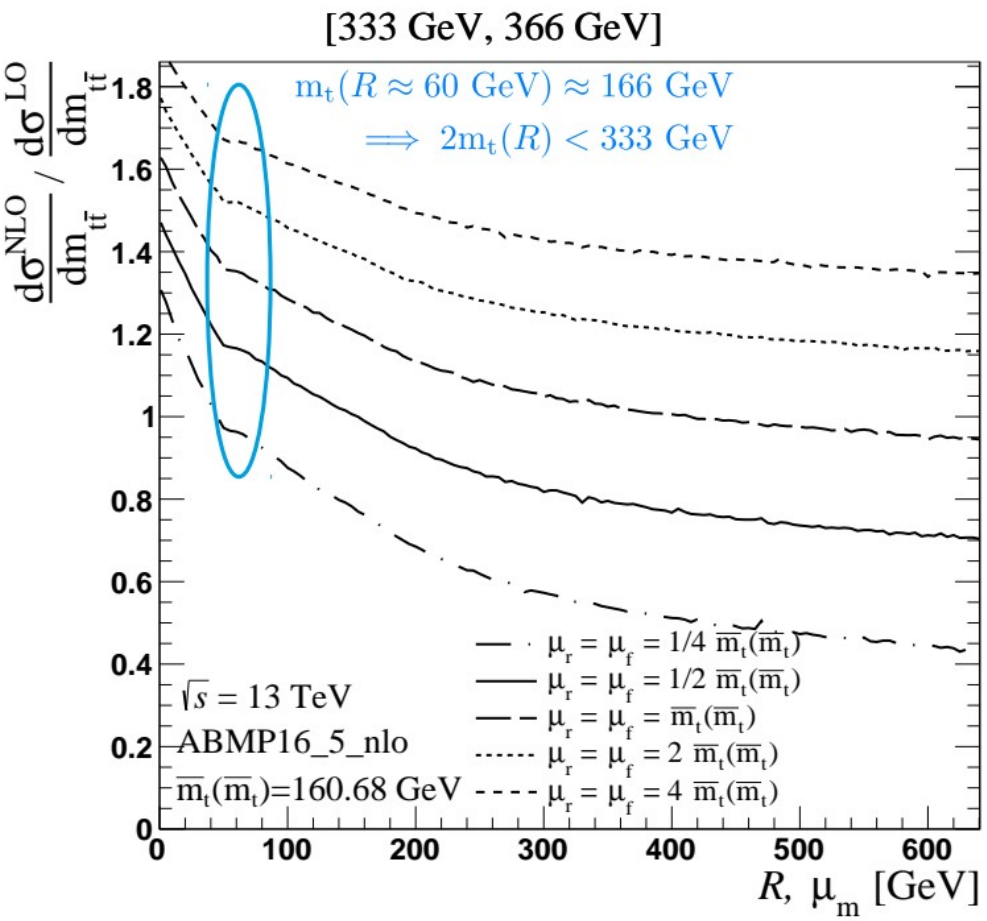

Studies of μ_r, μ_f and *R* behavior in $d\sigma/dm_{t\bar{t}}$ at NLO

- With the fine binning, the two lowest lowest $m_{t\bar{t}}$ bins indicate the regions suffering from missing Coulomb corrections

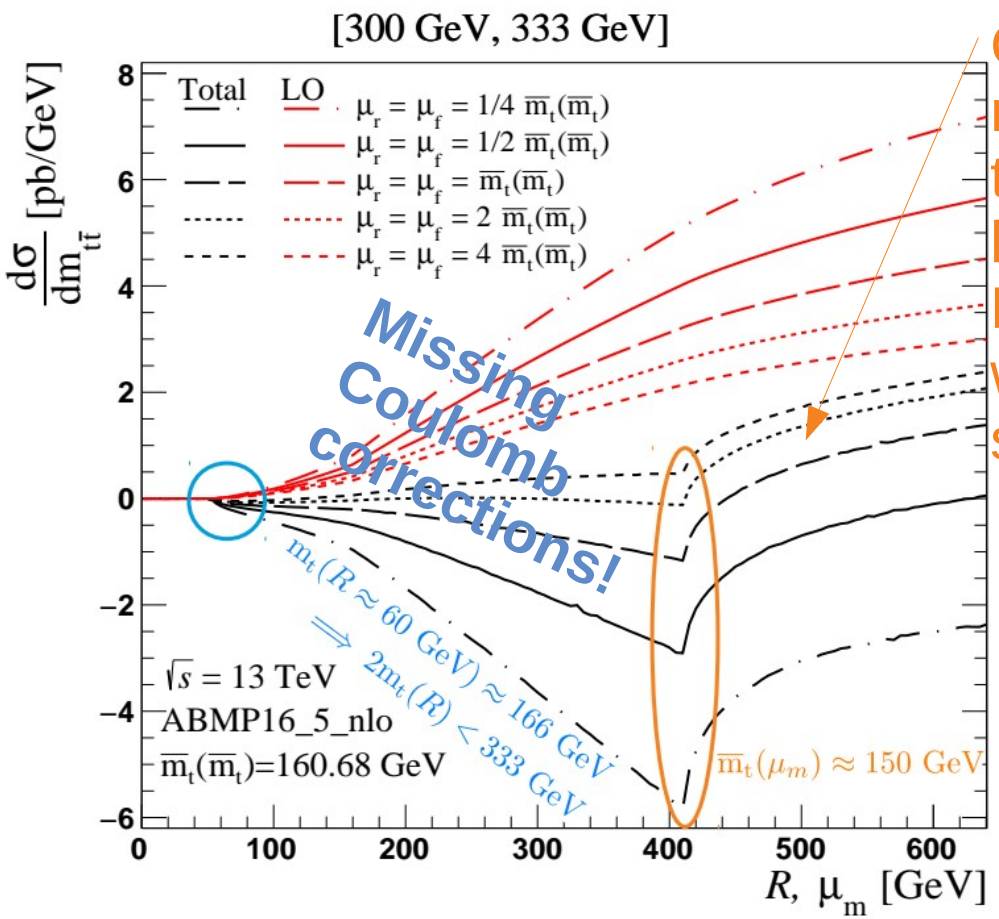

Cross section gets non-negative, when threshold is below the bin lower boundary. However, very high μ_m would be an artificial solution

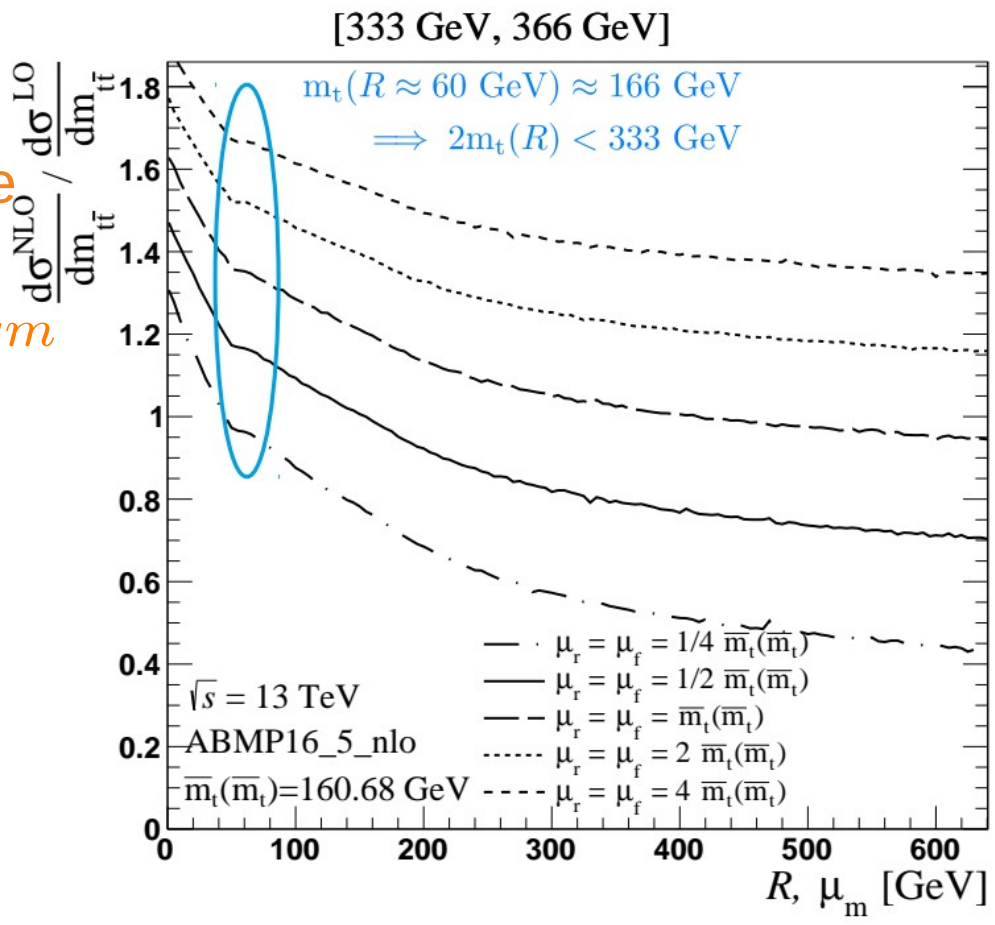

Studies of μ_r, μ_f and *R* behavior in $d\sigma/dm_{t\bar{t}}$ at NLO

- With the fine binning, the two lowest lowest $m_{t\bar{t}}$ bins indicate the regions suffering from missing Coulomb corrections

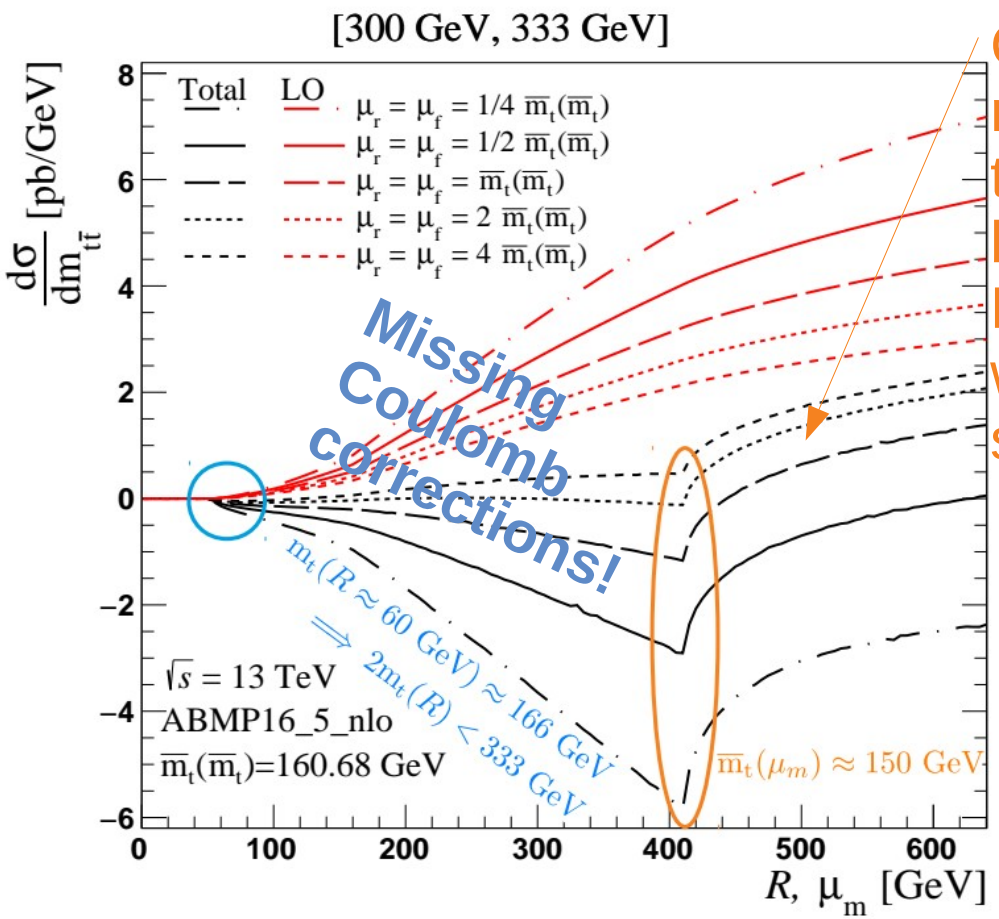

Cross section gets non-negative, when threshold is below the bin lower boundary. However, very high μ_m would be an artificial solution

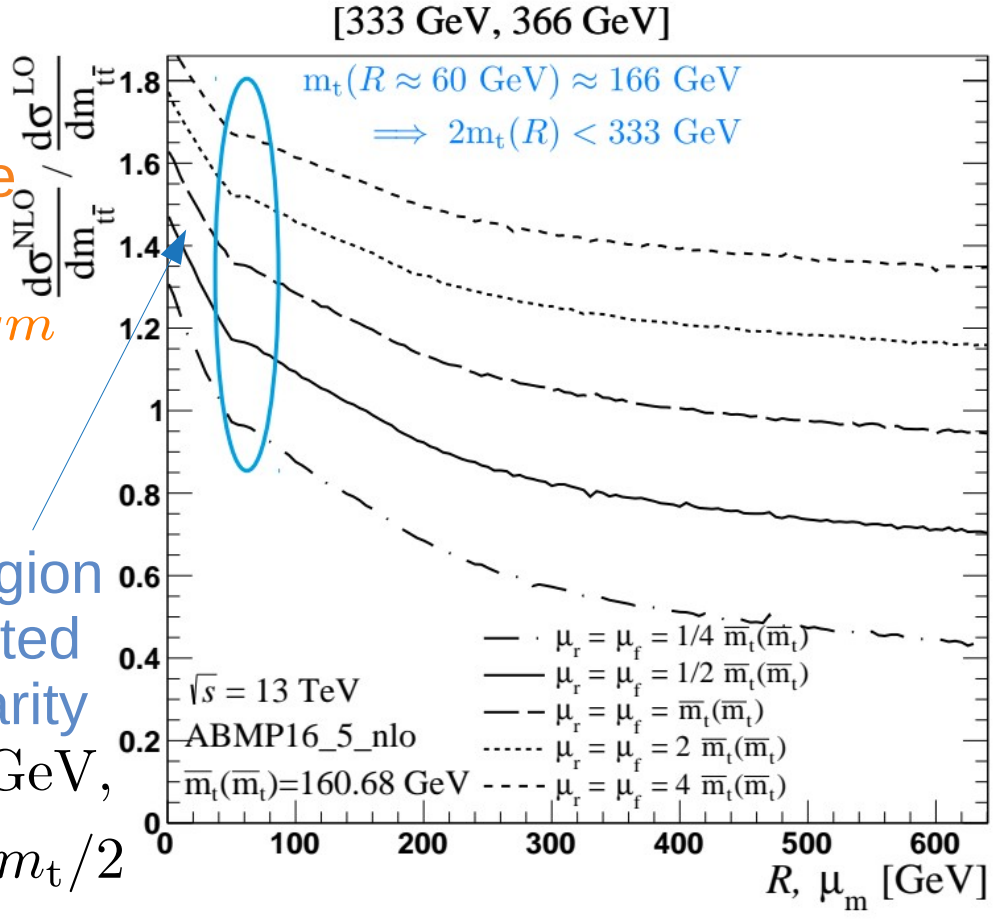

Analogously, the region below this still affected by Coulomb singularity

→ Use $R > 60\ \text{GeV}$,

e.g. $R = 80\ \text{GeV} \approx m_t/2$

Extraction m_t^{MSRn} from CMS data at 13 TeV

- Extracted the CMS data from *Running of the top quark mass from proton-proton collisions at 13 TeV* [doi:10.1016/j.physletb.2020.135263]

- Set *R*=80 GeV, scan for $m_{\mathrm{t}}^{\mathrm{MSR}}(80\ \mathrm{GeV})$
  - For each mass, compute

$$\chi^2 = \sum_{i,j} (\mu_i - m_i) C_{ij}^{-1} (\mu_j - m_j)$$

- Examine different scale choice options in different bins, also dynamical scales

- The plot illustrates one step in the scan with equal scales for all bins

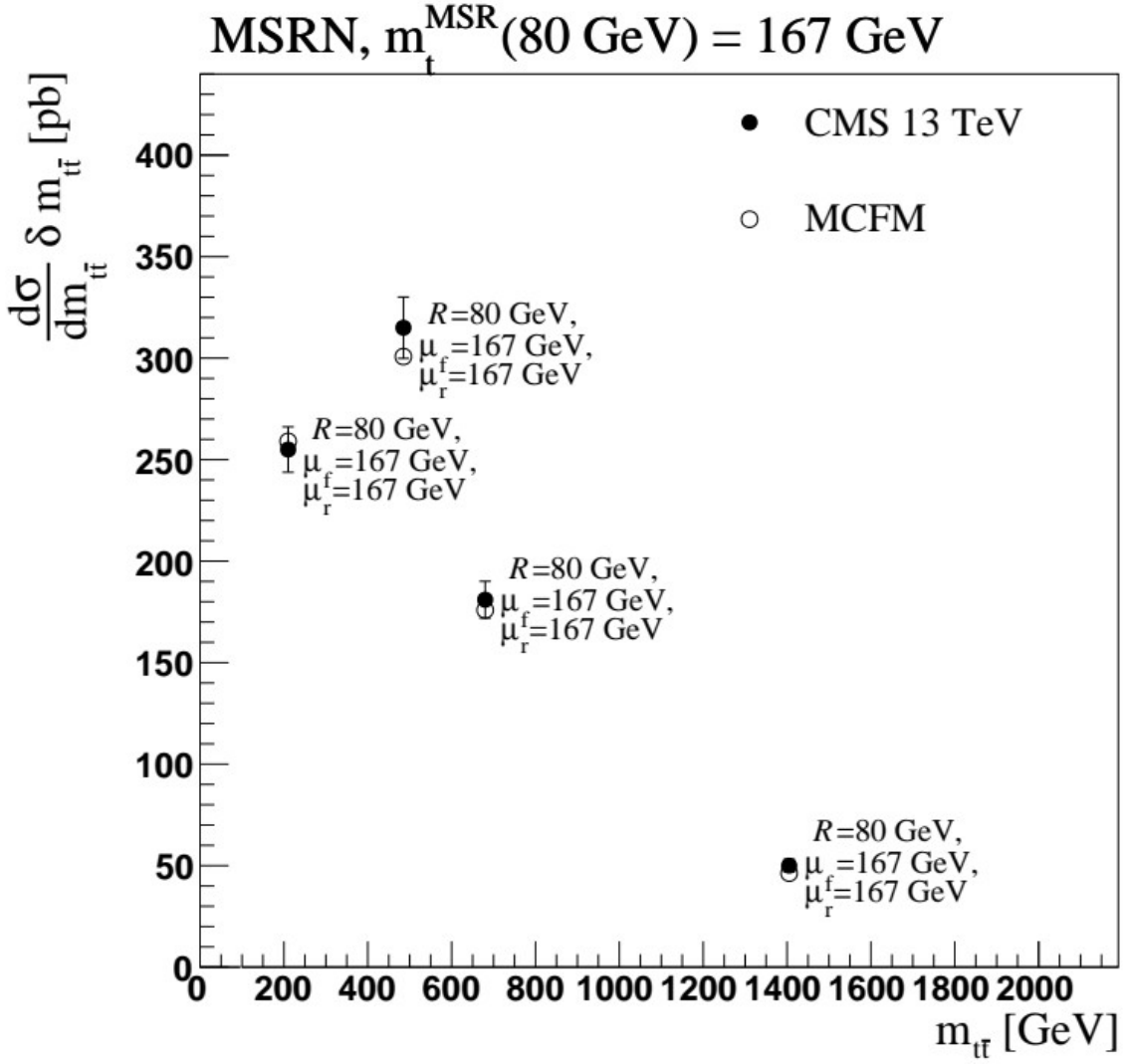

Extraction m_t^{MSRn} from CMS data at 13 TeV

- A 4rd order polynomial is fitted to the χ^2, fit uncertainties are obtained via $\Delta\chi^2 = 1$
- Scale uncertainties from varying $\mu_r^{(i)},\ \mu_f^{(i)}$ in each bin *i* by $2^{\pm 1}$, avoiding cases taking $\mu_r^{(i)}/\mu_f^{(i)} \to 4^{\pm 1}\mu_r^{(i)}/\mu_f^{(i)}$
- Evolve extracted $m_{\mathrm{t}}^{\mathrm{MSR}}(80\ \mathrm{GeV})$ to $m_{\mathrm{t}}^{\mathrm{MSR}}(1\ \mathrm{GeV})$, $m_{\mathrm{t}}^{\mathrm{MSR}}(2\ \mathrm{GeV})$ and $\overline{m}_{\mathrm{t}}(\overline{m}_{\mathrm{t}})$ (with matching) for reference
- *R*-uncertaninty is obtained by reperforming the fits with $R = 60\ \mathrm{GeV}$ and $R = 100\ \mathrm{GeV}$, then taking the difference of the masses evolved to the reference scales

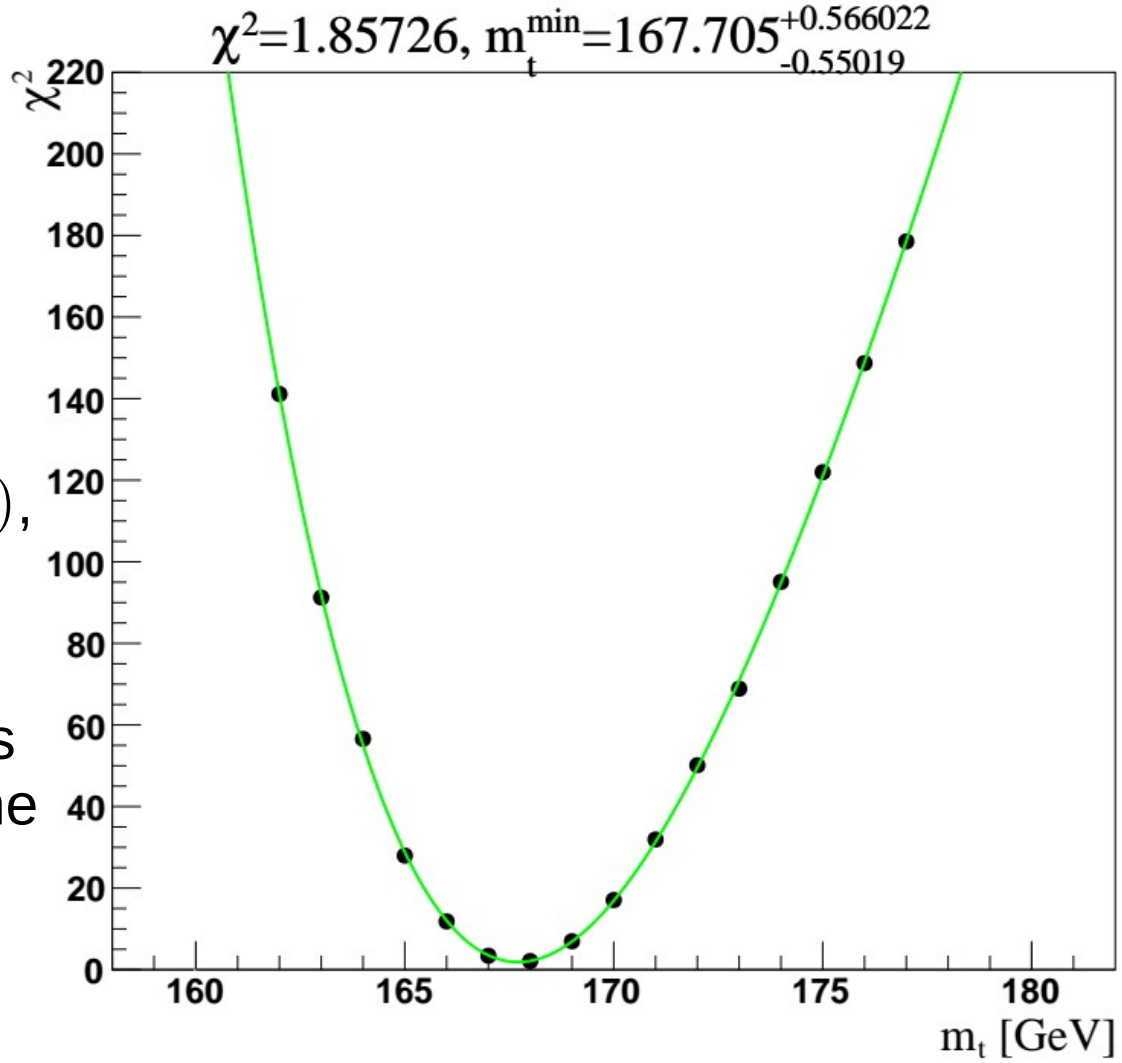

Extraction m_t^{MSRn} from CMS data at 13 TeV

- Additional fits are performed by...

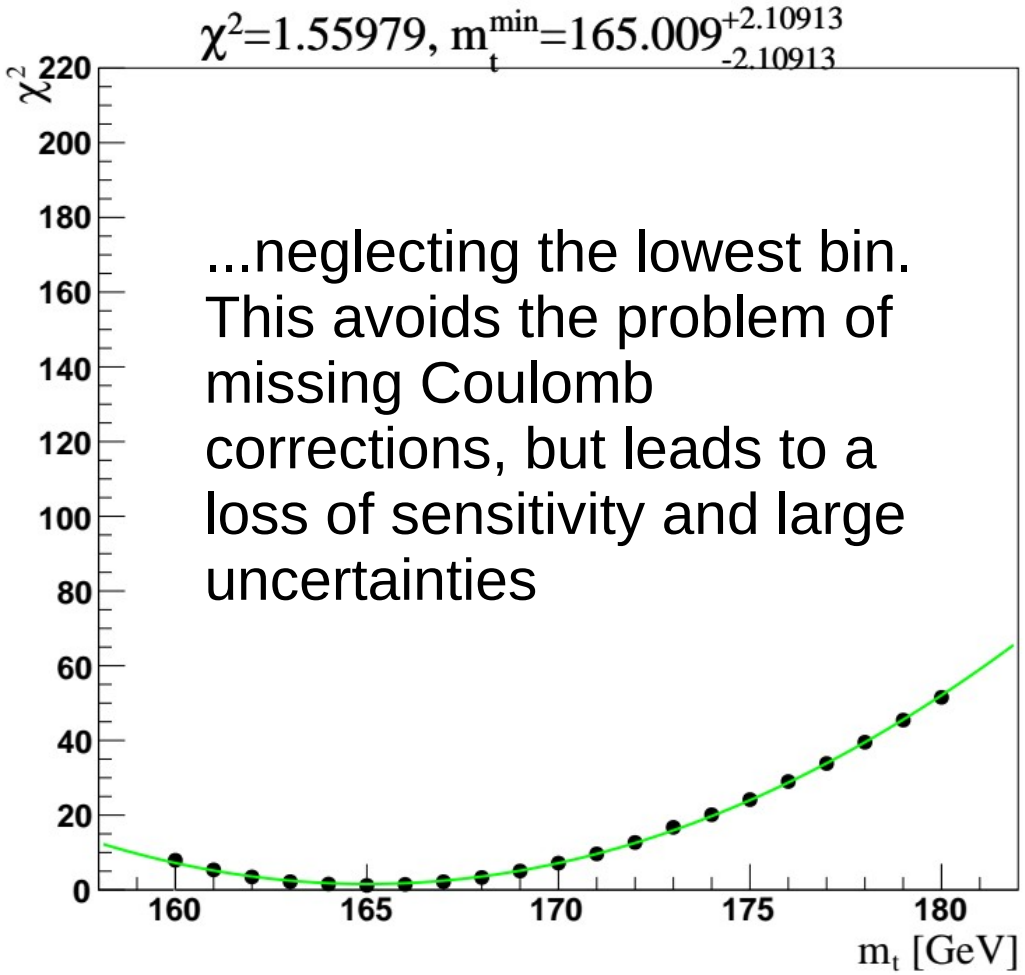

...neglecting the lowest bin. This avoids the problem of missing Coulomb corrections, but leads to a loss of sensitivity and large uncertainties

Extraction m_t^{MSRn} from CMS data at 13 TeV

- Additional fits are performed by...

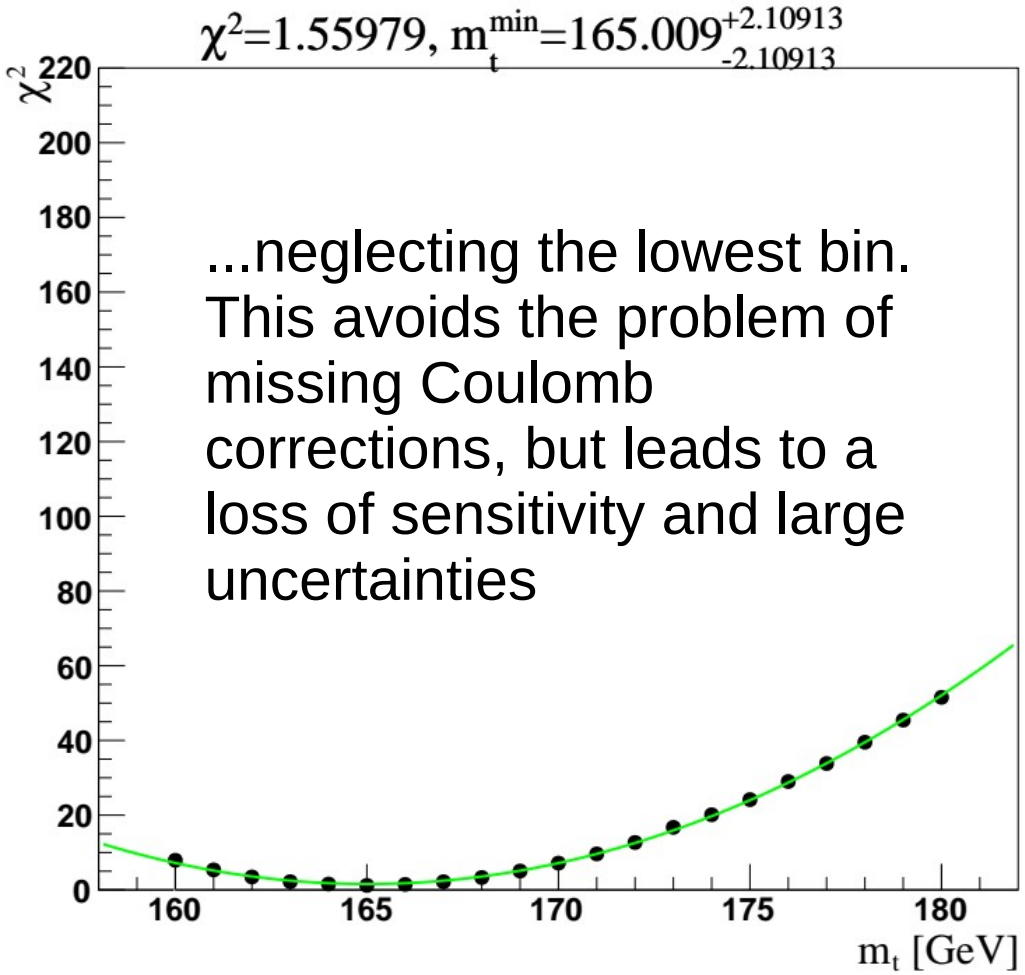

...neglecting the lowest bin. This avoids the problem of missing Coulomb corrections, but leads to a loss of sensitivity and large uncertainties

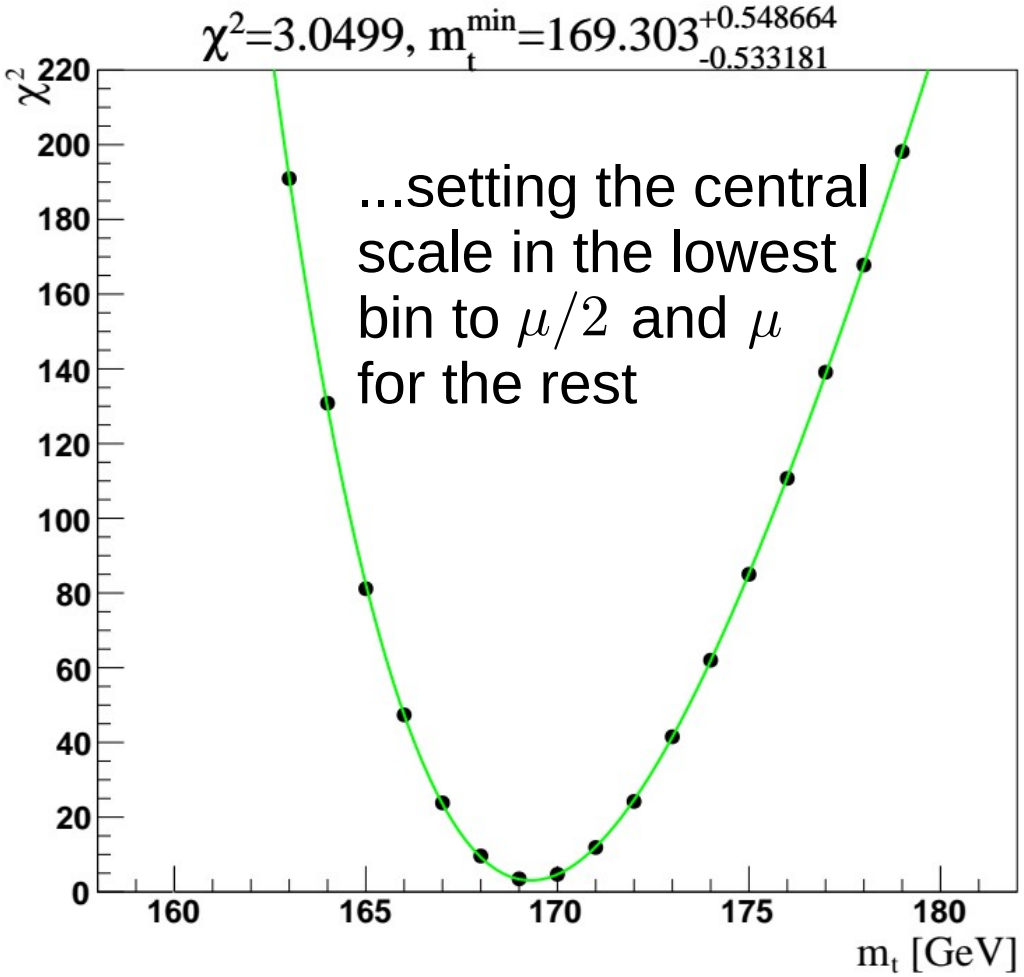

...setting the central scale in the lowest bin to $\mu/2$ and μ for the rest

Extraction m_t^{MSRn} from CMS data at 13 TeV

Mass goes up, compensates for the increase in the cross section in the lowest bin

- Additional fits are performed by...

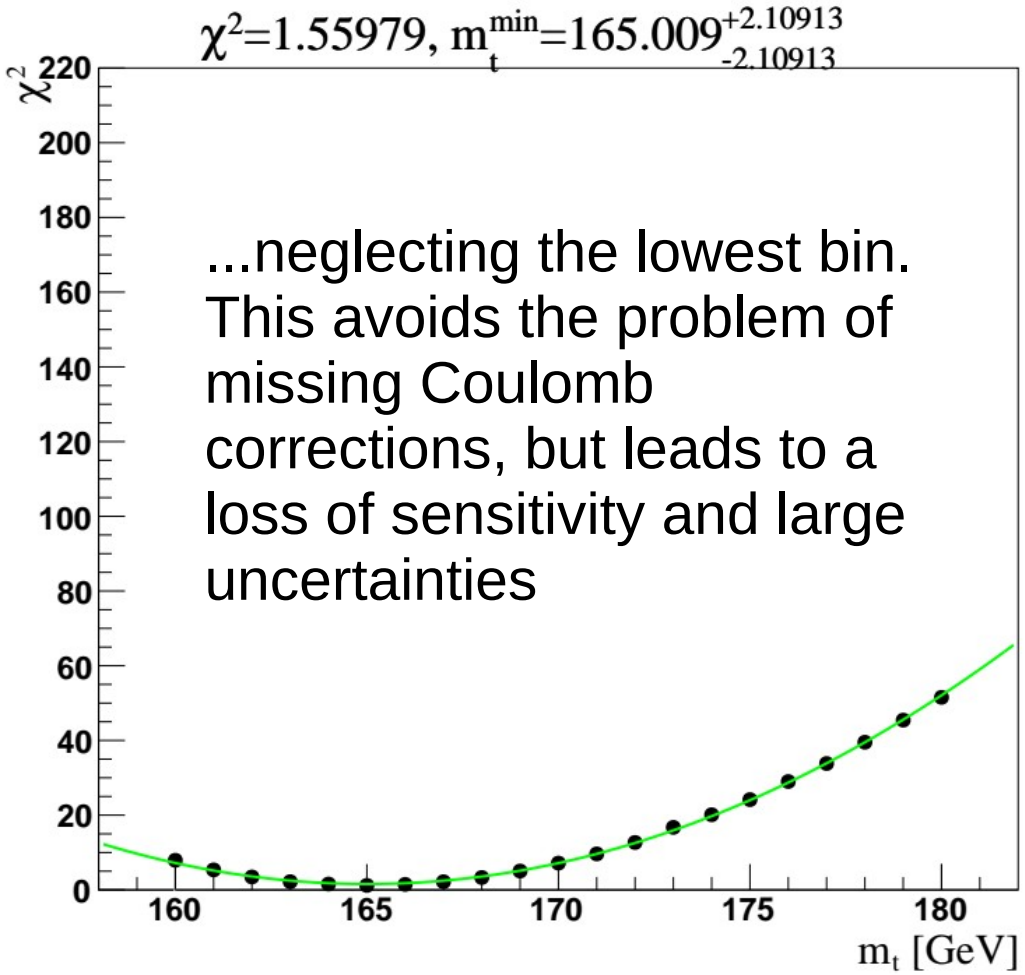

...neglecting the lowest bin. This avoids the problem of missing Coulomb corrections, but leads to a loss of sensitivity and large uncertainties

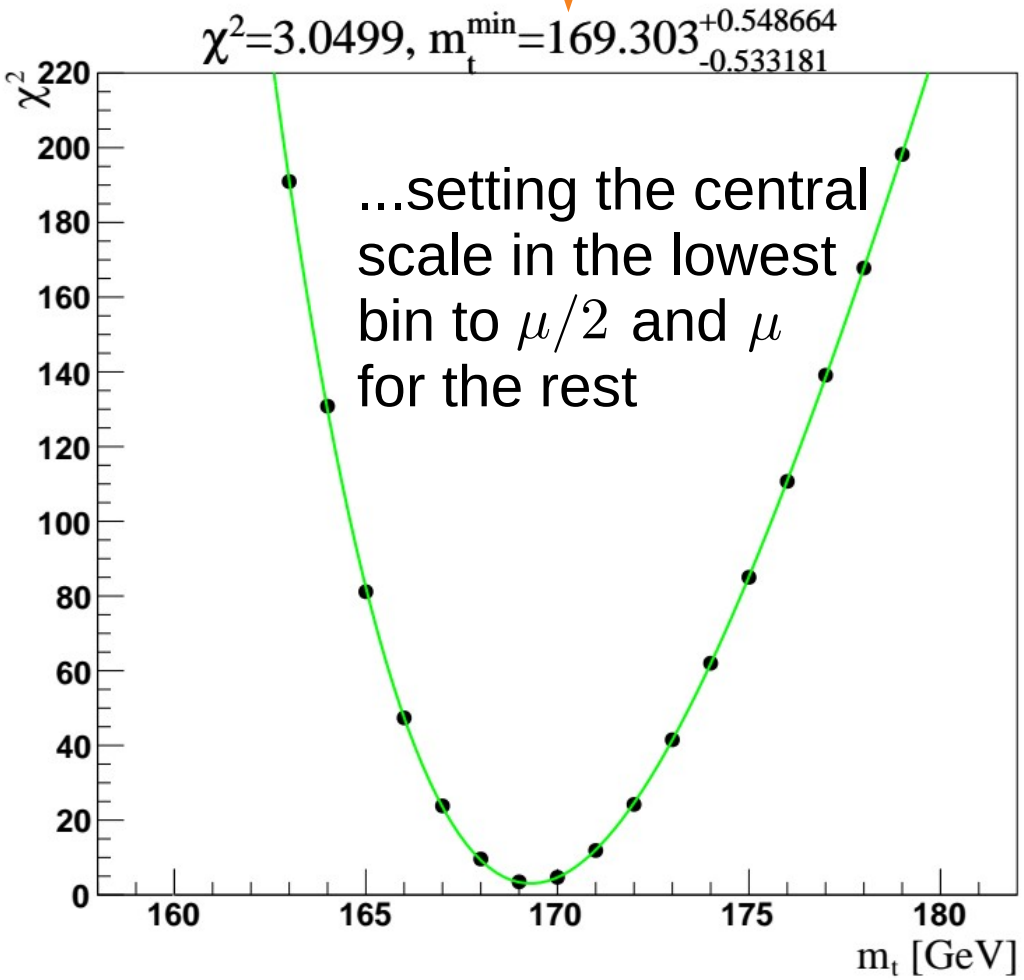

...setting the central scale in the lowest bin to $\mu/2$ and μ for the rest

Extraction m_t^{MSRn} from CMS data at 13 TeV

	$\mathrm{m_t^{MSR}}(80)$ [GeV]	$\mathrm{m_t^{MSR}}(1)$ [GeV]	$\mathrm{m_t^{MSR}}(2)$ [GeV]	$\overline{m}_{\mathrm{t}}(\overline{m}_{\mathrm{t}})$ [GeV]	Fit [GeV]	(μ_r, μ_f) [GeV]	(R) [GeV]
(μ, μ, μ, μ)	167.7	173.2	173.0	163.3	$^{+0.6}_{-0.6}$	$^{+0.4}_{-0.6}$	$^{+0.4}_{-0.5}$
$(-, \mu, \mu, \mu)$	165.0	170.5	170.3	160.7	$^{+2.1}_{-2.1}$	$^{+6.7}_{-9.8}$	$^{+0.5}_{-0.5}$
$(\frac{\mu}{2}, \mu, \mu, \mu)$	169.3	174.8	174.6	164.8	$^{+0.5}_{-0.5}$	$^{+0.2}_{-0.4}$	$^{+0.2}_{-0.3}$

- The fit and $\mu_r,\ \mu_f$ uncertainties correspond to the MSRn mass extracted at *R*=80 GeV
- Within the reported accuracy, the *R* uncertainty is the same for the evolution to all reference values

Extraction m_t^{MSRn} from CMS data at 13 TeV

	$\mathrm{m_t^{MSR}}(80)$ [GeV]	$\mathrm{m_t^{MSR}}(1)$ [GeV]	$\mathrm{m_t^{MSR}}(2)$ [GeV]	$\overline{m}_{\mathrm{t}}(\overline{m}_{\mathrm{t}})$ [GeV]	Fit [GeV]	(μ_r, μ_f) [GeV]	(R) [GeV]
(μ, μ, μ, μ)	167.7	173.2	173.0	163.3	$^{+0.6}_{-0.6}$	$^{+0.4}_{-0.6}$	$^{+0.4}_{-0.5}$
$(-, \mu, \mu, \mu)$	165.0	170.5	170.3	160.7	$^{+2.1}_{-2.1}$	$^{+6.7}_{-9.8}$	$^{+0.5}_{-0.5}$
$(\frac{\mu}{2}, \mu, \mu, \mu)$	169.3	174.8	174.6	164.8	$^{+0.5}_{-0.5}$	$^{+0.2}_{-0.4}$	$^{+0.2}_{-0.3}$

- The fit and $\mu_r,\ \mu_f$ uncertainties correspond to the MSRn mass extracted at *R*=80 GeV
- Within the reported accuracy, the *R* uncertainty is the same for the evolution to all reference values

- The values obtained in ATL-PHYS-PUB-2021-034:

$$\mathrm{POWHEG+PYTHIA8}: \ m_t^{\mathrm{MSR}}(1\ \mathrm{GeV}) = 172.42 \pm 0.1\ \mathrm{GeV}$$

$$\mathrm{POWHEG+HERWIG7}: \ m_t^{\mathrm{MSR}}(1\ \mathrm{GeV}) = 172.27 \pm 0.09\ \mathrm{GeV}$$

Agreement with (μ, μ, μ, μ) case w/in our uncertainties

- The $\overline{\mathrm{MS}}$ value in [doi:10.1016/j.physletb.2020.135263] agrees with the evolved (μ, μ, μ, μ) result within uncertainties

Extraction m_t^{MSRn} from CMS data at 13 TeV

	$\mathrm{m_t^{MSR}}(80)$ [GeV]	$\mathrm{m_t^{MSR}}(1)$ [GeV]	$\mathrm{m_t^{MSR}}(2)$ [GeV]	$\overline{m}_\mathrm{t}(\overline{m}_\mathrm{t})$ [GeV]	Fit [GeV]	(μ_r, μ_f) [GeV]	(R) [GeV]
(μ, μ, μ, μ)	167.7	173.2	173.0	163.3	$^{+0.6}_{-0.6}$	$^{+0.4}_{-0.6}$	$^{+0.4}_{-0.5}$
$(-, \mu, \mu, \mu)$	165.0	170.5	170.3	160.7	$^{+2.1}_{-2.1}$	$^{+6.7}_{-9.8}$	$^{+0.5}_{-0.5}$
$(\frac{\mu}{2}, \mu, \mu, \mu)$	169.3	174.8	174.6	164.8	$^{+0.5}_{-0.5}$	$^{+0.2}_{-0.4}$	$^{+0.2}_{-0.3}$

- The fit and $\mu_r,\ \mu_f$ uncertainties correspond to the MSRn mass extracted at *R*=80 GeV
- Within the reported accuracy, the *R* uncertainty is the same for the evolution to all reference values

N.B. dynamical scale brings scale uncertainties down!

- The values obtained in ATL-PHYS-PUB-2021-034:

$$\mathrm{POWHEG{+}PYTHIA8}: \ m_t^{\mathrm{MSR}}(1\ \mathrm{GeV}) = 172.42 \pm 0.1\ \mathrm{GeV}$$

$$\mathrm{POWHEG{+}HERWIG7}: \ m_t^{\mathrm{MSR}}(1\ \mathrm{GeV}) = 172.27 \pm 0.09\ \mathrm{GeV}$$

Agreement with (μ, μ, μ, μ) case w/in our uncertainties

- The $\overline{\mathrm{MS}}$ value in [doi:10.1016/j.physletb.2020.135263] agrees with the evolved (μ, μ, μ, μ) result within uncertainties

Summary

- MSRn and MSRp schemes are now implemented into HATHOR 2.0 and MCFM v6.8, and the codes are validated
  - Single-differential cross section predictions in bins of $m_{t\bar{t}}$, $p_{\mathrm{T}}(\bar{t})$ and $y(\bar{t})$
- Studying the three scales independent of each other suggests that lower $\mu_r,\ \mu_f$ values stabilize the predictions as a function of *R*, especially close to the threshold
  - Using a dynamical scale can bring all scale uncertainties down
- An extraction of the MSR mass is performed, which is consistent with previous MSR results but includes additional analysis of the uncertainties
  - Also consistent with the $\overline{\mathrm{MS}}$ result from the corresponding CMS publication
- Next step: a full understanding of the threshold region will require Coulomb corrections and matching to the fixed-order result from MCFM

Thanks for your attention!